Unraveling the Absorption Spectra of Alkali Metal Atoms Attached to Helium Nanodroplets†

Oliver Bünermann,*,‡ Georg Droppelmann,§ Alberto Hernando,# Ricardo Mayol,# and Frank Stienkemeier‡

Physikalisches Institut, Universität Freiburg, Hermann-Herder-Strasse 3, 79104 Freiburg, Germany, Fakultät für Physik, Universität Bielefeld, Universitätsstrasse 25, 33615 Bielefeld, Germany, and Departament ECM, Facultat de Física, and IN²UB, Universitat de Barcelona, Diagonal 647, 08028 Barcelona, Spain

Received: July 31, 2007; In Final Form: October 16, 2007

The absorption spectra of the first electronic exited state of alkali metal atoms on helium nanodroplets formed of both ^{4}He and ^{3}He isotopes were studied experimentally as well as theoretically. In the experimental part new data on the 2p ← 2s transition of lithium on ^{3}He nanodroplets are presented. The absorption spectrum changes drastically when compared to ^{4}He droplets, in contrast to sodium where only marginal differences were observed in former studies. To explain these large differences and to answer some still open questions concerning the interaction of alkali metal atoms with helium nanodroplets, a model calculation was performed. New helium density profiles as well as a refined model allowed us to achieve good agreement with the experimental findings. For the first time the red-shifted intensities in the lithium and sodium spectra are explained in terms of enhanced binding configurations in the excited state displaced spatially from the ground state configurations.

I. Introduction

Helium nanodroplets form a unique size-limited quantum aggregate with fascinating properties. In spite of their very low equilibrium temperature of only a few 100 mK[1] they are fluid. ^{4}He droplets even show the properties of a superfluid and droplets made of the isotope ^{3}He remain normal fluid in that temperature range.[2] The droplets can easily be loaded with a vast number of atoms and molecules via pick-up from the gas phase, making helium nanodroplet isolation spectroscopy (HENDI) a powerful spectroscopic tool.[3,4] Besides their advantages as a spectroscopic matrix, helium nanodroplets are very interesting on their own, forming a quantum system on the nano scale.[5]

Doping helium nanodroplets with alkali metal atoms forms a peculiar situation compared to adding other atoms or molecules. Theoretical calculations predict a well depth in the alkali metal atom−helium pair interaction potential of ≈2 wave numbers.[6−8] Kleinekathöfer et al. showed in their work,[9] that for all alkali metal atoms a bound state with very long binding length should exist, but until now this could not be confirmed experimentally. However, it was shown that the alkali metal atoms are weakly (≈10 cm^{-1}) bound to helium nanodroplets.[10−13] They reside in a dimple on the surface of the droplets in contrast to nearly all other dopants that submerge to the center of the droplets. This makes alkali metal atoms a potential probe for surface excitations of helium nanodroplets. Recently, experiments and theoretical calculations with droplets formed of ^{3}He doped with alkali metal atoms have been performed. They showed that the location of the sodium atoms is quite similar for both isotopes.[14,15] However, the absorption spectra show peculiar differences. Although all stable alkali metal atoms were studied experimentally and theoretically, there are still unsolved questions concerning the interaction between the droplets and the alkali metal atoms.

Figure 1 shows the absorption profiles of the first excited state of the alkali metal atoms on ^{4}He nanodroplets. They are plotted over energy subtracted by the energy of the D_1 atomic line. The first absorption as well as emission spectra of lithium, sodium, and potassium were recorded by Stienkemeier et al.[11] In respect to the atomic lines, lithium exhibits a red-shifted asymmetric line. Even further red-shifted, a small shoulder is found in the spectrum (marked with arrow). The line shape of the sodium spectrum is similar, but it is slightly blue-shifted and wider. Here also a red-shifted shoulder is observed. In the case of potassium the stronger spin−orbit coupling leads to a splitting of the lines. Additionally, no absorption red-shifted to the atomic lines has been recorded. The emission spectra in conjunction with a theoretical model led to the result that the absorption is composed of different contributions. They differ in an alignment of the p-orbital in the excited state with respect to the surface of the droplet. An alignment perpendicular to the surface leads to a Π state, one horizontal to the surface to a Σ state. Upon excitation of a Σ state the atom desorbs from the droplet (bound−continuum transition) and only emission of free atoms can be recorded in the experiment. After exciting a Π state a bound state (bound−bound transition) is formed and red-shifted emission is observed. The red-shifted shoulder found in the experiment in the case of lithium and sodium could not be explained within their model.[11]

The rubidium spectrum has first been recorded by Brühl et al.[12] Because of the larger spin−orbit coupling, one observes two completely separated lines. The D_1 line shows a broad slightly asymmetric profile. The D_2 line has more transition strength and shows a wide blue shoulder. The splitting of the D_2 line was assigned to Π and Σ contributions. With the help

† Part of the "Giacinto Scoles Festschrift".

* Corresponding author. E-mail: oliver.buenermann@physik.uni-freiburg.de.

‡ Universität Freiburg.

§ Universität Bielefeld.

Universitat de Barcelona.

10.1021/jp0760760 CCC: $37.00
Published on Web 11/13/2007

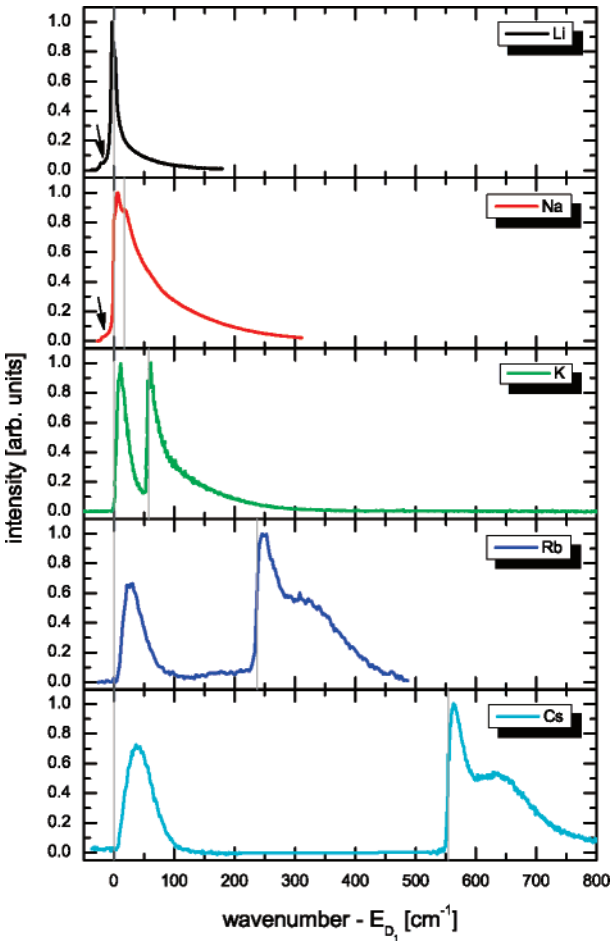

Figure 1. Absorption spectra of the s to p transition of the alkali metal atoms Li, Na, K, Rb, and Cs on ^{4}He nanodroplets.[11,13] The energies are plotted relative to the atomic D_1 line. The gray vertical lines represent the atomic transitions. See text for further details.

of emission spectroscopy the red-shifted emission upon excitation of the Π state was attributed to exciplex formation: an alkali metal−helium molecule is formed that eventually desorbs from the droplet. Relaxation to the ground state results in red-shifted emission intensities and fragmentation.

The 6p ← 6s transition of cesium was recorded before in our work group.[13] Cesium showed qualitatively the same absorption profile as rubidium. As a new method resonant two-photon ionization was used, which enabled us to count the ions mass selectively and allowed us to directly decompose the spectra into different contributions. This method revealed that the $\Pi_{3/2}$ state is further split.

Recent experiments on ^{3}He droplets studied the influence of the selection of isotopes on the absorption spectra.[14,15] The fact that ^{4}He droplets are superfluid but ^{3}He are normal fluid gives the possibility to extract the influence of superfluidity on the spectra. The experiments revealed that sodium is also bound in a dimple on the surface of the ^{3}He droplets. The absorption spectra are very similar for both isotopes, but the red-shifted shoulder is missing in the case of ^{3}He.

The interaction of helium with alkali metal atoms has also been studied in the bulk in different aggregate states. Comparing these results with the ones obtained in helium droplets gives further hints for the interpretation of the spectra. In the case of rubidium and cesium, measurements in liquid helium exist. In the case of the lighter alkali metal atoms, no data in liquid helium are available because the emission is strongly quenched.[16] The absorption of rubidium and cesium is much more blue-shifted in liquid helium than on helium nanodroplets,[17] confirming the surface location on nanodroplets. The shift was explained within the bubble model. A splitting of the D_2 line was observed and assigned to the dynamic Jahn−Teller-Effect,[18] a possible candidate for the observed splitting of the $\Pi_{3/2}$ contribution on helium nanodroplets. Alkali metal atoms additionally were investigated in dense helium gas via emission spectroscopy.[19−21] The observed features in the emission spectra were explained in the framework of exciplex formation. Furthermore, cesium was studied in solid helium.[22,23] Finally, also rubidium has been studied in solid helium. Emission intensities were nearly completely quenched, like those for the lighter alkali metal atoms in liquid helium.[24]

Alkali metal atoms attached to helium nanodroplets have also been studied via time-resolved methods, providing an alternative promising method to reveal couplings of alkali metal atoms to surface or volume modes of droplets. In particular, the exciplex formation was the focus of these experiments. The formation times of sodium[25] and potassium[27] exciplexes were determined by time correlated single photon counting. Furthermore, the technique of femtosecond pump−probe spectroscopy was used to measure the formation times of potassium[28] and rubidium[29] exciplexes. Comparing the formation times for both helium isotopes provided evidence that the cooling efficiency of the droplet plays an important role in these processes.

In summary, despite a significant amount of data, the spectra are not fully understood and no satisfying theoretical description of the alkali metal atom−helium nanodroplet system exist. One unsolved question is the origin of the red-shifted shoulder in the absorption of lithium and sodium on ^{4}He droplets. Moreover, in the case of sodium even the assignment of the different peaks of the spectrum is not clear: fine structure or Π and Σ contributions of the spectrum. A further question is the reason for the splitting of the $\Pi_{3/2}$ line observed experimentally for cesium.

In this paper, a refined model to calculate the electronic transitions of the dopant alkali metal using realistic density profiles for the helium droplets of both isotopes enables us to answer most of the open questions. These profiles are needed to properly describe the alkali metal−helium droplet interaction. Profiles of droplets of up to 5000 helium atoms have been used. These sizes are comparable to the experimental droplet sizes. Additionally, we present experimental results for the spectroscopy of lithium on ^{3}He droplets to further support the presented simulation and interpretations.

II. Experiment

The experiments were performed in a helium droplet machine applying laser-induced fluorescence (LIF) as well as beam depletion (BD) spectroscopy. A detailed description of the experimental setup is presented elsewhere.[30] Modifications include a new droplet source to reach the lower temperatures needed for generating ^{3}He droplets.[14] In short, gas of either helium isotope is expanded under supersonic conditions from a nozzle, forming a beam of droplets traveling freely in high vacuum. The helium stagnation pressure in the droplet source is 20 bar, and a nozzle of 5 μm diameter has been used. The nozzle temperature has been stabilized to 12 and 15 K to form ^{3}He and ^{4}He droplets, respectively. These conditions result in an average droplet size of $\approx$5000 helium atoms.[3]

The droplets are doped downstream using the pickup technique: in a heated scattering cell, an appropriate vapor pressure of lithium is established so droplets pick up one single atom on average when passing the cell. LIF as well as BD absorption

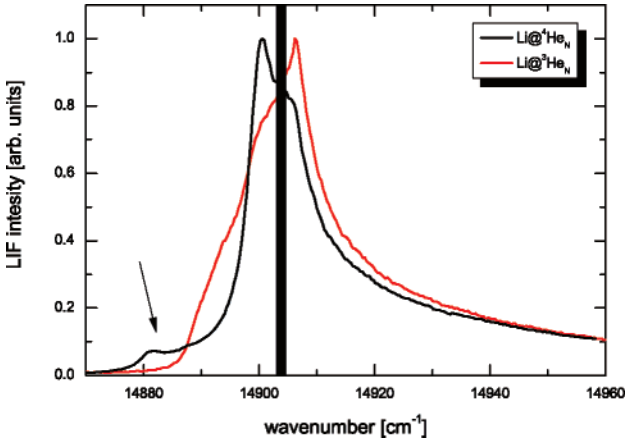

Figure 2. Absorption spectrum of the 2p ← 2s transition of lithium on ^{3}He nanodroplets compared to that on ^{4}He nanodroplets.[11] The black bar covers the atomic lines.

spectra of the doped droplet beam can be recorded upon electronic excitation using a cw dye laser. LIF is recorded with a photo multiplier tube. For the beam depletion measurement, a Langmuir−Taylor surface ionization detector has been used.[31]

Here, only the results obtained using LIF are shown as a better signal-to-noise ratio was achieved when compared to the BD spectra for lithium doped clusters. However, the BD measurements show identical results when compared to the LIF spectra.

Figure 2 shows the absorption spectra of the 2p ← 2s transition of lithium on droplets of both helium isotopes. In contrast to sodium, where both spectra are quite similar, the spectra in the case of lithium differ strongly. Only the line width is comparable. An interpretation of the different line forms will be given in the theoretical part of the paper.

III. Theoretical Model

The model to simulate the absorption spectra is based on the use of pair interaction potentials calculated by Pascale[6] and of alkali-doped helium density profiles obtained within density functional theory using the He−alkali metal potentials calculated by Patil.[7] Some technical details about the calculation of the nanodroplet structure can be found in our recent work on doped helium droplets.[5,15,32] The heavier alkali metals have been treated as an external potential, neglecting their zero point motion. For the lighter Na and Li cases, we have solved the Euler−Lagrange and Schrödinger equations that result from the variations of the density functional that describes the droplet-impurity complex, thus taking into account the quantal character of the dopant atom.

The reason to use Pascale's potentials to obtain the atomic shifts is the availability of ground and excited state pair potentials covering all helium−alkali metal pairs. Pascale's potentials do not include the spin−orbit (SO) interaction. For the heavier alkali metal atoms, the SO coupling is relevant and it has been taken into account as described below. More recent pair potential calculations have been done for specific, single impurities (lithium,[33] sodium,[34] potassium[35]).

Due to the general lacking of excited states for He−alkali metal potentials, we have obtained the crucial dimple structure using Patil potentials but have then employed the corresponding density profile in conjunction with the Pascale ground and excited state potentials to generate the atomic shifts. We want to point out that we have ruled out the obvious possibility of using Pascale potentials to obtain the ground state of the droplet as well as the atomic shifts because these potentials are too

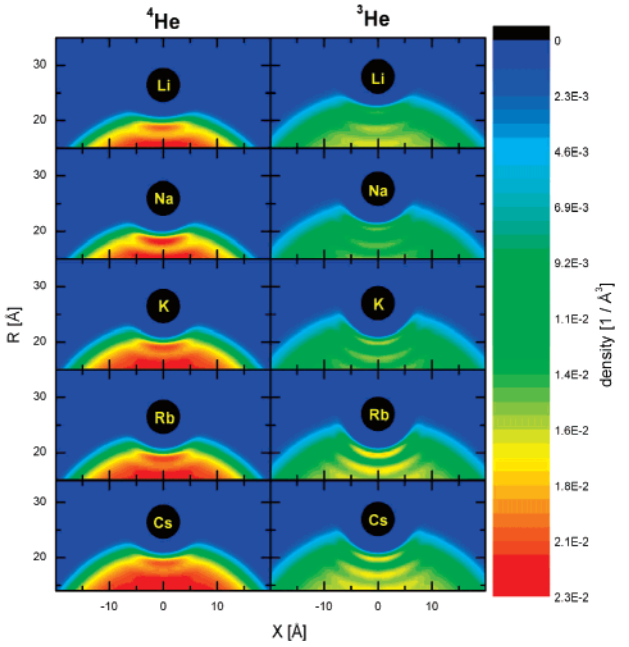

Figure 3. Density profiles of ^{3}He and ^{4}He nanodroplets with $N = 1000$ atoms doped with alkalis.

attractive as compared with the more recent ones, thus yielding too a deep dimple and, hence, an unrealistic atomic shift. This strategy has turned out to be a reasonable one in view of the obtained results but clearly indicates that the main limitation to theoretically describe the shifts is the nonavailability of reliable He−impurity pair potentials.

Figure 3 shows a section of the density of helium nanodroplets made of $N = 1000$ atoms for both isotopes doped with the five stable alkali metal atoms. The false color legend is similar for both isotopes for the sake of comparison. The heavier the alkali metal atom, the deeper the dimple. The dimples are deeper for ^{3}He than for ^{4}He. It is worth noting the overall lower density of ^{3}He. These facts have a major influence on the resulting spectra in the simulation.

To obtain the droplet−alkali metal atom interaction potentials, we have followed an approach similar to that of Stienkemeier et al.,[11] but now using 3-dimensional droplet density profiles matching experimental conditions and considering the orientation of the orbital of the alkali metal atom relative to the helium atoms of the droplet. We consider the system as a diatomic molecule, with the alkali metal acting as one atom and the droplet acting as another. The droplet density is kept frozen while the excitation takes place (Franck−Condon principle). Because we are only interested in calculating the absorption spectra, this assumption is fully justified, as the electronic motion is an order of magnitude faster than that of the helium atoms. Therefore, the model does not give information on the time evolution of the system. For this reason we cannot reproduce the right line shape, because line broadening mechanisms are not included. To include inhomogeneous broadening resulting from droplet size distribution, the line width of the laser, and similar effects, we have convoluted the calculated lines with a Gaussian profile with fwhm 5 cm^{-1}. The interaction potential is calculated by folding the helium density with the interaction pair potentials, namely,

$$V_{\mathrm{A\ on\ He_N}}(n\Lambda, \vec{R}) - V_{\mathrm{A}}(nl) = \int [V_{\mathrm{AHe}}(n\Lambda, \vec{R}-\vec{R}') - V_{\mathrm{A}}(nl)]\rho_{\mathrm{He}}(\vec{R}')\,\mathrm{d}\vec{R}' \quad (1)$$

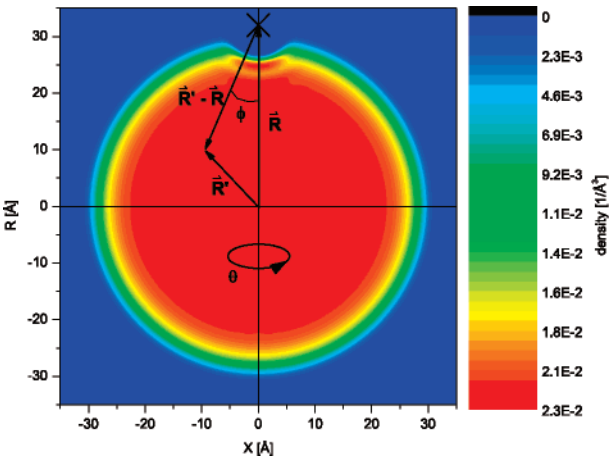

Figure 4. Illustration of the coordinate system. The droplet corresponds to the Na(^{4}He$_{5000}$) complex.

A represents the particular alkali metal atom, n the principle quantum number, V_{AHe} the pair potential with Λ the projection of the angular momentum onto the "molecule axis", V_A the potential of the alkali metal atom, and l the angular momentum quantum number. Three-body interaction effects and effects of higher order are neglected. Figure 4 illustrates the used coordinate system. In the two-body case, there are two possibilities for the first electronic excited state. They differ in the alignment of the p-orbital with respect to the helium atom. In the horizontal alignment, the projection of the angular momentum is 0 and the state is called Σ. A perpendicular alignment results in a Π state. We have chosen as the quantization axis the line connecting the alkali metal atom and the center of the droplet. Therefore, most of the helium density is not located on this axis but "sees" the alkali metal atom at an angle. One finds the helium density up to an angle of 60°. When calculating the folding, one has to take into account the relative orientations. To describe a state that is quantized in a rotated coordinate system, Alexander et al. have developed an approach based on rotation operators.[36] If one rotates the coordinate system, the angular momentum eigenvectors are transformed into a linear combination of those in the rotated frame. The formulas can be found, e.g., in Zare's book.[38]

$$|JM'\rangle = \mathbf{R}^{-1}(\phi,\theta,\chi)|JM\rangle = \sum_{M'} D^J_{MM'}(\phi,\theta,\chi)|JM'\rangle \quad (2)$$

The expansion coefficients $D^J_{MM'}$ are the elements of the rotation matrix **R**, and ϕ, θ, and χ are the Euler angles of the rotation transformation. Strictly speaking, this formula is only valid for angular momentum eigenvectors $|JM\rangle$. But in the case of the alkali metal−helium interaction potential one can always assign an atomic angular momentum to the alkali metal atom; therefore this transformation can be applied. The rotation can be split into the separate rotations:

$$D^J_{MM'}(\phi,\theta,\chi) = e^{-i\phi M} d^J_{MM'}(\theta) e^{-i\chi M'} \quad (3)$$

The elements $d^J_{MM'}(\theta)$ are determined by

$$d^J_{MM'}(\theta) = [(J+M')!(J-M')!(J+M)!(J-M)!]^{1/2} \times \sum_\nu \frac{(-1)^\nu}{(J-M-\nu)!(J+M-\nu)!(\nu+M-M')!\nu!} \times \left[\cos\left(\frac{\theta}{2}\right)\right]^{2J+M'-M-2\nu} \left[-\sin\left(\frac{\theta}{2}\right)\right]^{M-M'+2\nu} \quad (4)$$

The rotation can be straightforwardly applied to the Hamiltonian, which becomes

$$\mathbf{H}' = \mathbf{R}\mathbf{H}\mathbf{R}^{-1} \quad (5)$$

The eigenvalues of $\mathbf{H}'$ and **H** are the same, as **R** is unitary, and the eigenvectors of $\mathbf{H}'$ and **H** are related by the above expression eq 2.

Lithium and sodium only show weak SO couplings, but one cannot neglect the SO interaction for the heavier alkali metal atoms. When incorporating SO in our model, one has to keep in mind that the rotation is only valid for eigenstates of the angular momentum. The pair potentials are diagonal in the uncoupled basis. But transforming these into the coupled basis leads to a matrix also containing off-diagonal elements. Opposite the SO coupling is diagonal in the coupled basis but not in the uncoupled one. This leads to the fact that the pair potentials transformed into the coupled basis are no longer eigenstates of the angular momentum operator. One can only combine both effects either when $V_\Pi - V_\Sigma \gg E_{SO}$ and one can neglect the SO interaction or when $V_\Pi - V_\Sigma \ll E_{SO}$ and one can neglect the off-diagonal elements of the potential matrix in the coupled basis, and in this way avoid mixing of different states. These terms depend on the internuclear distance. For alkali metal atoms, SO is prominent at large distances. When approaching the potential wells, $V_\Pi - V_\Sigma$ increases and becomes equal to or larger than the SO energy depending on the alkali metal atom. In our model we are only interested in the shape of the wells. We calculated $V_\Pi - V_\Sigma$ at the pair potential minimum of the ground state and compared this to the SO energy. If the SO energy is smaller, we neglect it for all distances, adding SO afterward via an appropriate displacement of the potentials. Otherwise, we incorporate the SO interaction but neglect the off-diagonal elements. This approach is justified, because the main contribution to the shifts results from the helium density in the direct vicinity of the alkali metal atom. The method introduced by Cohen and Schneider[37] cannot be used, because after applying the rotation one no longer has "pure" Σ and Π states. Hence, for lithium and sodium we have neglected the SO interaction, whereas for rubidium and cesium it has been considered. In the case of potassium both terms are comparable. Here we calculated the spectra with both approaches. It turned out that neglecting SO gives better agreement of the calculated spectra with the experimental result.

A. Uncoupled Basis. The Hamiltonian corresponding to the atomic p state in the uncoupled basis is

$$\mathbf{H} = \begin{pmatrix} V_\Pi & 0 & 0 \\ 0 & V_\Sigma & 0 \\ 0 & 0 & V_\Pi \end{pmatrix} \quad (6)$$

The rotation matrix is

$$\mathbf{R} = \begin{pmatrix} e^{-i\phi}\frac{1}{2}(1+\cos\theta)e^{-i\chi} & -e^{-i\phi}\sqrt{\frac{1}{2}}\sin\theta & e^{-i\phi}\frac{1}{2}(1-\cos\theta)e^{i\chi} \\ \sqrt{\frac{1}{2}}\sin\theta e^{-i\chi} & \cos\theta & -\sqrt{\frac{1}{2}}\sin\theta e^{i\chi} \\ e^{i\phi}\frac{1}{2}(1-\cos\theta)e^{-i\chi} & e^{i\phi}\sqrt{\frac{1}{2}}\sin\theta & e^{i\phi}\frac{1}{2}(1+\cos\theta)e^{i\chi} \end{pmatrix} \tag{7}$$

The transformed Hamiltonian H′ has the following form:

$$\mathbf{H}' = \begin{pmatrix} V_\Pi\cos^2\theta + \frac{1}{2}(V_\Pi + V_\Sigma)\sin^2\theta & \sqrt{\frac{1}{2}}e^{-i\phi}(V_\Pi - V_\Sigma)\cos\theta\sin\theta & \frac{1}{2}e^{-2i\phi}(V_\Pi - V_\Sigma)\sin^2\theta \\ \sqrt{\frac{1}{2}}e^{i\phi}(V_\Pi - V_\Sigma)\cos\theta\sin\theta & V_\Pi\sin^2\theta + V_\Sigma\cos^2\theta & -\sqrt{\frac{1}{2}}e^{-i\phi}(V_\Pi - V_\Sigma)\cos\theta\sin\theta \\ \frac{1}{2}e^{2i\phi}(V_\Pi + V_\Sigma)\sin^2\theta & -\sqrt{\frac{1}{2}}e^{i\phi}(V_\Pi - V_\Sigma)\cos\theta\sin\theta & V_\Pi\cos^2\theta + \frac{1}{2}(V_\Pi + V_\Sigma)\sin^2\theta \end{pmatrix} \tag{8}$$

This is the Hamiltonian matrix in the aligned basis for the interaction between the alkali metal atom and one helium atom in cylindrical coordinates. To calculate the interaction potential between the alkali metal atom and the helium droplet system, we use eq 1. Because the problem has azimuthal symmetry, one can carry out the integration over ϕ, which gives a 2π factor in eq 1. This results in a huge simplification of the potential matrix: All off-diagonal elements become zero and one can go on with the calculation with only the diagonal matrix elements:

$$V'_\Sigma(r,\theta) = V_\Sigma(r)\cos^2\theta + V_\Pi(r)\sin^2\theta \tag{9}$$

$$V'_\Pi(r,\theta) = V_\Pi(r)\cos^2\theta + \frac{1}{2}[(V_\Pi(r) + V_\Sigma(r)]\sin^2\theta) \tag{10}$$

B. Coupled Basis. In the case of rubidium and cesium the SO energy Δ_{SO} becomes dominant and one has to calculate the potentials in the coupled basis:

$$\mathbf{H} = \begin{pmatrix} V_\Pi + \Delta_{SO}/3 & 0 & 0 & 0 & 0 & 0 \\ 0 & \frac{1}{3}(V_\Pi + 2V_\Sigma + \Delta_{SO}) & \frac{1}{3}\sqrt{2}(V_\Pi - V_\Sigma) & 0 & 0 & 0 \\ 0 & \frac{1}{3}\sqrt{2}(V_\Pi - V_\Sigma) & \frac{1}{3}(2V_\Pi + V_\Sigma - 2\Delta_{SO}) & 0 & 0 & 0 \\ 0 & 0 & 0 & \frac{1}{3}(V_\Pi + 2V_\Sigma + \Delta_{SO}) & \frac{1}{3}\sqrt{2}(-V_\Pi + V_\Sigma) & 0 \\ 0 & 0 & 0 & \frac{1}{3}\sqrt{2}(-V_\Pi + V_\Sigma) & \frac{1}{3}(2V_\Pi + V_\Sigma - 2\Delta_{SO}) & 0 \\ 0 & 0 & 0 & 0 & 0 & V_\Pi + \Delta_{SO}/3 \end{pmatrix} \tag{11}$$

Off-diagonal elements have been neglected and thus one can extract the potential matrices for the $J = {}^1/_2$ and ${}^3/_2$ states:

$$\mathbf{H}_{1/2} = \begin{pmatrix} \frac{1}{3}(2V_\Pi + V_\Sigma - 2\Delta_{SO}) & 0 \\ 0 & \frac{1}{3}(2V_\Pi + V_\Sigma - 2\Delta_{SO}) \end{pmatrix} \tag{12}$$

$$\mathbf{H}_{3/2} = \begin{pmatrix} V_\Pi + \Delta_{SO}/3 & 0 & 0 & 0 \\ 0 & \frac{1}{3}(V_\Pi + 2V_\Sigma + \Delta_{SO}) & o & 0 \\ 0 & o & \frac{1}{3}(V_\Pi + 2V_\Sigma + 2\Delta_{SO}) & 0 \\ 0 & 0 & 0 & V_\Pi + \Delta_{SO}/3 \end{pmatrix} \tag{13}$$

The rotation matrices are

$$\mathbf{R}_{1/2} = \begin{pmatrix} e^{-(1/2)i\phi}\cos\frac{\theta}{2}e^{-(1/2)i\chi} & e^{-(1/2)i\phi}\sin\frac{\theta}{2}e^{(1/2)i\chi} \\ -e^{(1/2)i\phi}\sin\frac{\theta}{2}e^{-(1/2)i\chi} & e^{(1/2)i\phi}\cos\frac{\theta}{2}e^{(1/2)i\chi} \end{pmatrix} \tag{14}$$

$$\mathbf{R}_{3/2} = \begin{pmatrix} e^{-(3/2)i\phi}\cos^3\frac{\theta}{2}e^{-(3/2)i\chi} & -e^{-(3/2)i\phi}\sqrt{3}\cos^2\frac{\theta}{2}\sin\frac{\theta}{2}e^{-(1/2)i\chi} & e^{-(3/2)i\phi}\sqrt{3}\cos\frac{\theta}{2}\sin^2\frac{\theta}{2}e^{(1/2)i\chi} & -e^{-(3/2)i\phi}\sin^3\frac{\theta}{2}e^{(3/2)i\chi} \\ e^{-(1/2)i\phi}\sqrt{3}\cos^2\frac{\theta}{2}\sin\frac{\theta}{2}e^{-(3/2)i\chi} & e^{-(1/2)i\phi}\cos\frac{\theta}{2}\left(-2+3\cos^2\frac{\theta}{2}\right)e^{-(1/2)i\chi} & e^{-(1/2)i\phi}\sin\frac{\theta}{2}\left(-2+3\sin^2\frac{\theta}{2}\right)e^{(1/2)i\chi} & e^{-(3/2)i\phi}\sqrt{3}\cos\frac{\theta}{2}\sin^2\frac{\theta}{2}e^{(1/2)i\chi} \\ e^{(1/2)i\phi}\sqrt{3}\cos\frac{\theta}{2}\sin^2\frac{\theta}{2}e^{-(3/2)i\chi} & -e^{(1/2)i\phi}\sin\frac{\theta}{2}\left(-2+3\sin^2\frac{\theta}{2}\right)e^{-(1/2)i\chi} & e^{(1/2)i\phi}\cos\frac{\theta}{2}\left(-2+3\cos^2\frac{\theta}{2}\right)e^{(1/2)i\chi} & -e^{(3/2)i\phi}\sqrt{3}\cos^2\frac{\theta}{2}\sin\frac{\theta}{2}e^{(1/2)i\chi} \\ e^{(3/2)i\phi}\sin^3\frac{\theta}{2}e^{-(3/2)i\chi} & e^{(3/2)i\phi}\sqrt{3}\cos\frac{\theta}{2}\sin^2\frac{\theta}{2}e^{-(1/2)i\chi} & e^{(3/2)i\phi}\sqrt{3}\cos^2\frac{\theta}{2}\sin\frac{\theta}{2}e^{(1/2)i\chi} & e^{(3/2)i\phi}\cos^3\frac{\theta}{2}e^{(3/2)i\chi} \end{pmatrix} \tag{15}$$

Using them on the Hamiltonian yields the potential matrix aligned in the right quantization axis. It turns out that the $\Pi_{1/2}$ state is spherically symmetric

$$V_{\Pi_{1/2}} = \frac{1}{3}(2V_\Pi + V_\Sigma - 2\Delta_{SO}) \tag{16}$$

Both $J = {}^3/_2$ states have cylindrical symmetry and so one can carry out the integration over ϕ, which leads to a simplification of the matrix:

$$V_{\Pi_{3/2}} = \frac{1}{12}[3(3V_\Pi + V_\Sigma) + 3(V_\Pi - V_\Sigma)\cos 2\theta + 4\Delta_{SO}] \tag{17}$$

$$V_{\Sigma_{1/2}} = \frac{1}{12}[7V_\Pi + 5V_\Sigma + 3(-V_\Pi + V_\Sigma)\cos 2\theta + 4\Delta_{SO}] \tag{18}$$

IV. Results

Figure 5 shows the calculated potentials for cesium on a $^4He_{2000}$ nanodroplet. It also includes the cesium helium pair interaction potentials for comparison. The ground state has a well depth of 16 cm^{-1}, so cesium is bound to the droplet with a fairly large energy of 15 cm^{-1}. The resulting potentials for the first excited state are all repulsive. No bound state is found. This means that the cesium spectrum purely consists of bound−continuum transitions. Potassium and rubidium behave similarly to cesium, but for the lighter alkali metal atoms sodium and lithium, we have also found bound−bound transitions for the Π states. Figure 6 shows the obtained potentials for lithium. The Π state has a shallow potential well. Its position is nearly the same as that of the ground state well. This leads to a direct bound−bound transition. The experiment revealed that after Π excitation also for the heavier alkalis the formation of an exciplex molecule can be observed.[12,13,26] This finding is not in conflict with the presented model. An excited alkali metal atom can still attract single helium atoms in its nodal plane, only the total interaction with all helium atoms of the droplet at the instance of excitation (ground state configuration) is repulsive.

To compare the simulated potentials with the available experimental data, the Franck−Condon factors were calculated using the program Level 8.0[39] or BCount 2.2[40,41] from R. J. Le Roy. To get the right proportions of the different contributions, the electronic degeneracy factor, the Höhn−London factor as well as the density of states for the bound−continuum transitions were incorporated.

The calculated spectra for cesium on droplets of either isotope are presented in Figure 7. For ^4He the experimental spectrum is included for comparison. With the help of resonant two-photon ionization, the spectrum could be decomposed into the excitations that lead to exciplex formation and these leading to desorption of single atoms. These contributions can be assigned to the $\Sigma_{1/2}$ and $\Pi_{3/2}$ states, respectively.

In the ^4He case, the calculated spectrum fits well the experiment. The $\Pi_{1/2}$ and $\Sigma_{1/2}$ contributions are only slightly shifted, the $\Pi_{1/2}$ state 8 cm^{-1} to the blue and the $\Sigma_{1/2}$ state 7 cm^{-1} to the red. They show the same profile as the experimental spectra. The $\Pi_{3/2}$ part is also only slightly blue-shifted (6 cm^{-1}) but the shape of the profile does fit the experimental findings very well. The experiment showed that the $\Pi_{3/2}$ transition is composed of at least two pieces. This splitting is not reproduced in the presented theory. A possible explanation of the splitting is the presence of a dynamic Jahn−Teller effect, which leads to the splitting of the D_2 line of cesium in liquid helium.[18] The lower panel of Figure 7 displays the result for ^3He droplets. The spectrum is qualitatively the same. All constituents are blue-shifted with respect to ^4He ($\Pi_{1/2}$, 13 cm^{-1}; $\Pi_{3/2}$, 25 cm^{-1}; $\Sigma_{1/2}$, 2 cm^{-1}). The $\Pi_{3/2}$ line is broader compared to the ^4He case.

We have obtained a similar picture for rubidium. Figure 8 shows the results of the simulation in comparison with the experimental spectrum. All states are blue-shifted ($\Pi_{1/2}$, 20 cm^{-1}; $\Pi_{3/2}$, 12 cm^{-1}; $\Sigma_{1/2}$, 35 cm^{-1}). The shape of the D_1 line is nicely reproduced, but again the D_2 line does not fit well. The unconsidered splitting of the $\Pi_{3/2}$ state might be the reason. Changing of He isotope leads to the same effects as seen for cesium. The profiles are blue-shifted ($\Pi_{1/2}$, 22 cm^{-1}; $\Pi_{3/2}$, 40 cm^{-1}; $\Sigma_{1/2}$, 6 cm^{-1}) and the $\Pi_{3/2}$ is broadened.

The spectra of potassium on helium droplets are presented in Figure 9. Here the line profiles of the simulation and the experiment match quite well. Again, one finds a blue shift of the simulated spectrum ($\Pi_{1/2}$, 3 cm^{-1}; $\Pi_{3/2}$, 11 cm^{-1}; $\Sigma_{1/2}$, 8 cm^{-1}). To fit the D_2 line, the transition strength to the blue of the $\Pi_{3/2}$ state is missing in the simulation. This might again indicate the mentioned further

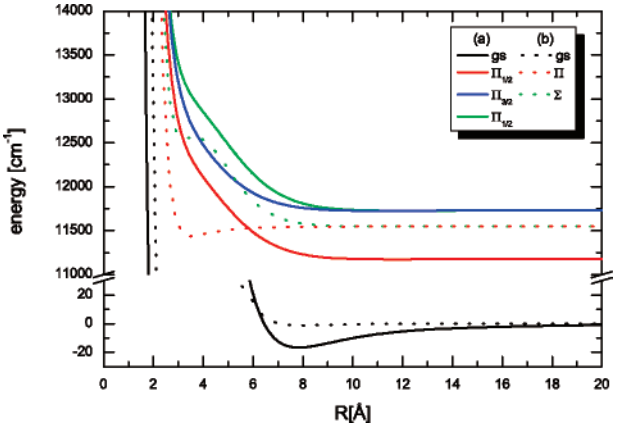

Figure 5. Simulated potentials for cesium bound to (a) a ^{4}He nanodroplet of size 2000. (b) Cesium helium pair potential.[6]

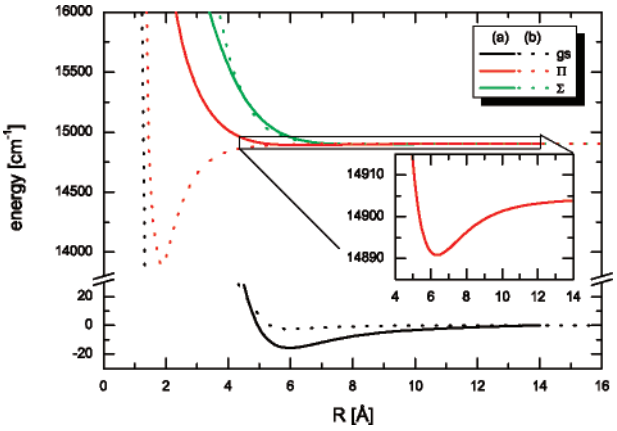

Figure 6. Simulated potentials for lithium bound to a (a) ^{4}He nanodroplet of size 5000. (b) Lithium helium pair potentials.[6]

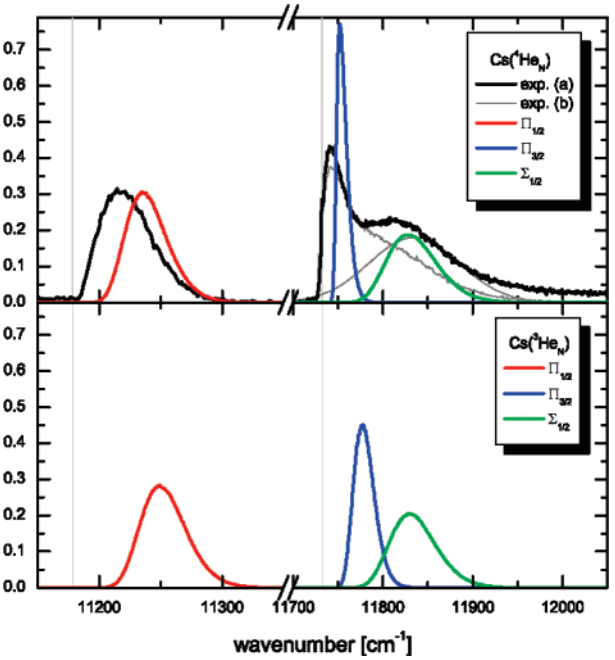

Figure 7. Simulated absorption profiles of the 6p ← 6s transition of cesium on ^{4}He$_{2000}$ and ^{3}He$_{2000}$ nanodroplets in comparison to experiment (exp): (a) integral spectrum, exp; (b) spectrum selective to Π and Σ contributions.[13]

mechanism that leads to a splitting of the $\Pi_{3/2}$ transition. In the case of potassium attached to ^{3}He droplets the line shape of both Π states changes notably. Besides a quite large blue shift

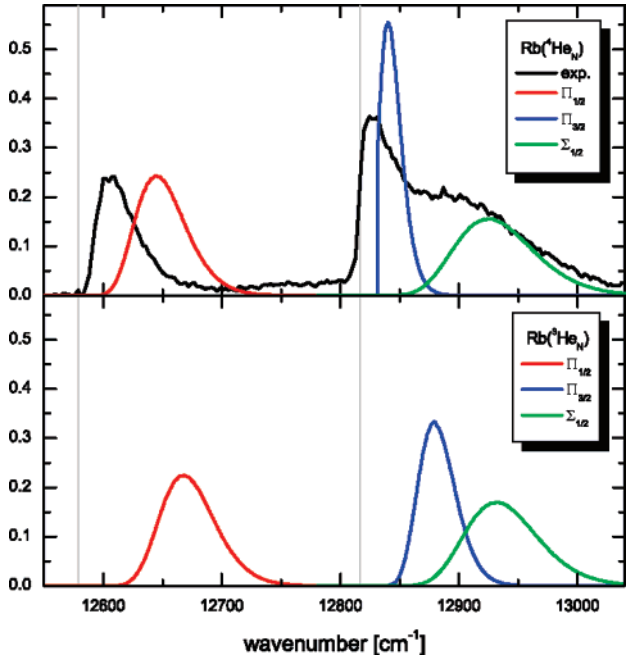

Figure 8. Simulated absorption profiles of the 5p ← 5s transition of rubidium on ^{4}He$_{2000}$ and ^{3}He$_{2000}$ nanodroplets, respectively, in comparison to experimental results.[12]

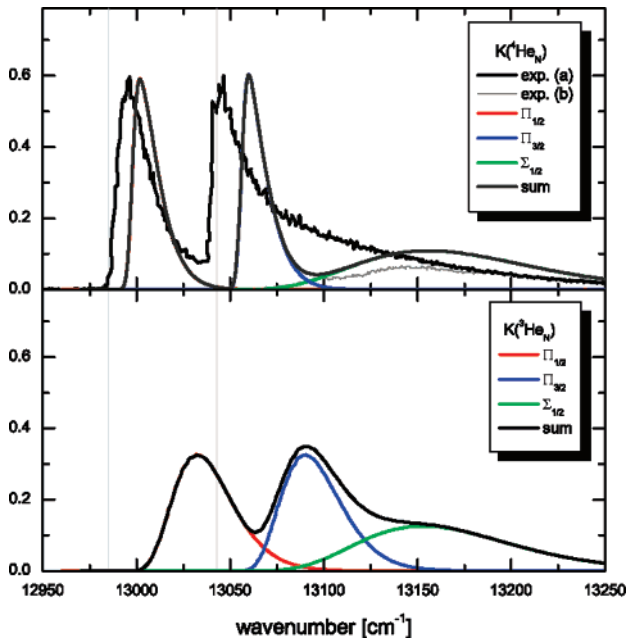

Figure 9. Simulated absorption profiles of the 4p ← 4s transition of potassium on ^{4}He$_{1500}$ and ^{3}He$_{2000}$ nanodroplets in comparison to experiment (exp): (a) integral spectrum, exp; (b) Σ part of the spectrum.[11]

($\Pi_{1/2}$, 34 cm^{-1}; $\Pi_{3/2}$, 33 cm^{-1}), the width of the line increases from 13 to 38 cm^{-1}. However, the $\Sigma_{1/2}$ state remains nearly the same.

For sodium, experimental data are available for both isotopes. Additionally, in the case of ^{4}He measurements of the different contributions via emission spectroscopy exist. These are plotted with the simulated spectrum in Figure 10. In contrast to previous calculations,[11] the sodium spectrum consists mainly of bound−continuum transitions and not of bound−bound ones. The transition into the Π states comes out to be partly bound−bound and partly bound−continuum. The main transition strength still arises from the bound−continuum part. All simulated profiles

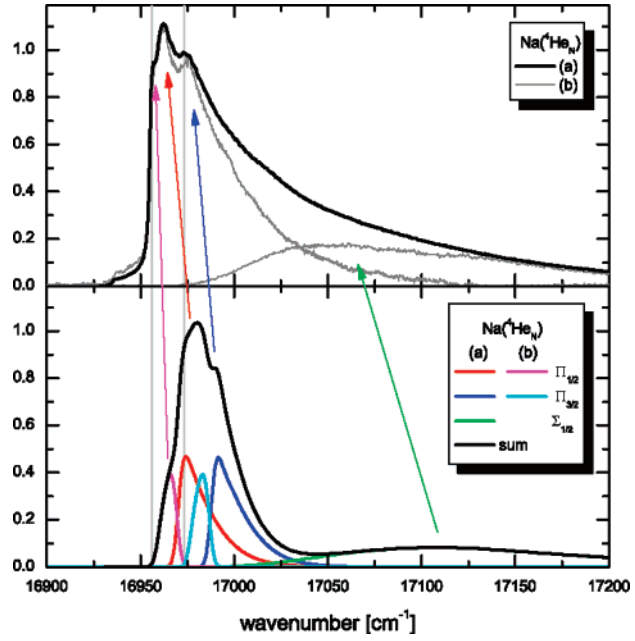

Figure 10. Simulated absorption profiles of the 3p ← 3s transition of sodium on $^4He_{5000}$ nanodroplets in comparison to experiment. Upper panel: (a) integral spectrum; (b) spectra assigned to Π and Σ contributions.[11] Lower panel: (a) bound−continuum part; (b) bound−bound part.

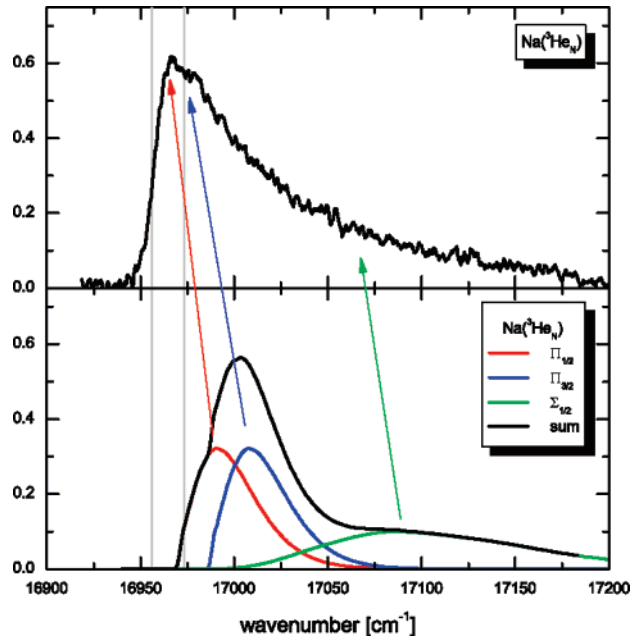

Figure 11. Simulated absorption profiles of the 3p ← 3s transition of sodium on $^3He_{5000}$ nanodroplets in comparison to experiment.[14]

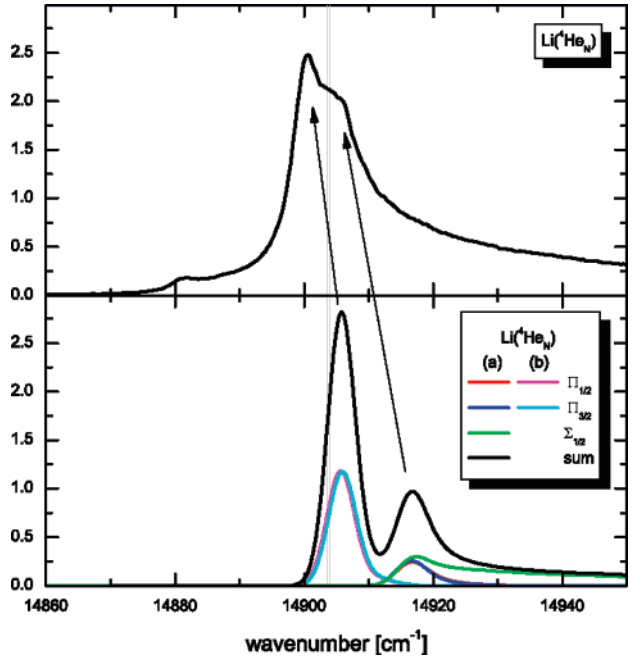

Figure 12. Simulated absorption profiles of the 2p ← 2s transition of lithium on $^4He_{5000}$ nanodroplets in comparison to experiment:[11] (a) bound−continuum part; (b) bound−bound part.

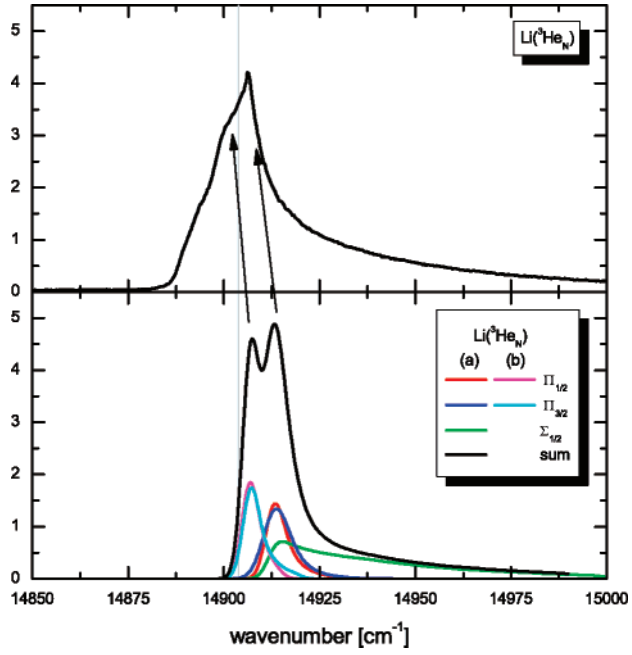

Figure 13. Simulated absorption profiles of the 2p ← 2s transition of lithium on $^3He_{5000}$ nanodroplets in comparison to experiment: (a) bound−continuum part; (b) bound−bound part.

are again blue-shifted ($\Pi_{1/2}$, 13 cm^{-1}; $\Pi_{3/2}$, 18 cm^{-1}; $\Sigma_{1/2}$, 46 cm^{-1}). Adding all the contributions achieves a nice agreement with the experiment. The three features in the maximum of the profile can be assigned to the bound−bound part of the $\Pi_{1/2}$ transition, the bound−bound part of the $\Pi_{3/2}$ plus the bound−continuum part of the $\Pi_{1/2}$ transition, and the bound−continuum part of the $\Pi_{3/2}$ transition. The red shoulder in the spectrum is not found in this simulation. Again, some transition strength in the blue of the $\Pi_{3/2}$ is missing, which leads once more to the conclusion that the $\Pi_{3/2}$ may be perturbed by a not included mechanism.

Going on to sodium on ^{3}He droplets, the simulation reveals that in this case no bound−bound transitions participate. Figure 11 shows both spectra in comparison. Unfortunately, the experimental spectrum cannot be decomposed into its contributions. Only the position of the $\Pi_{1/2}$ state is clear. Here, we also find a blue shift, in this case of about 25 cm^{-1}. When looking at the sum of the simulated parts, one gets again an incorrect profile, leading to the same conclusion as before. The simulated ^{3}He spectrum is 16 cm^{-1} blue-shifted with respect to the simulated ^{4}He spectrum. Experimentally, a shift of 7.5 cm^{-1} was found. This means that our simulation yields the gross feature but overestimates the amount by a factor of 2.

The last alkali metal atom we have studied is lithium. In the case of lithium the experiments show that the Π transition is red-shifted with respect to the atomic lines. This suggests that

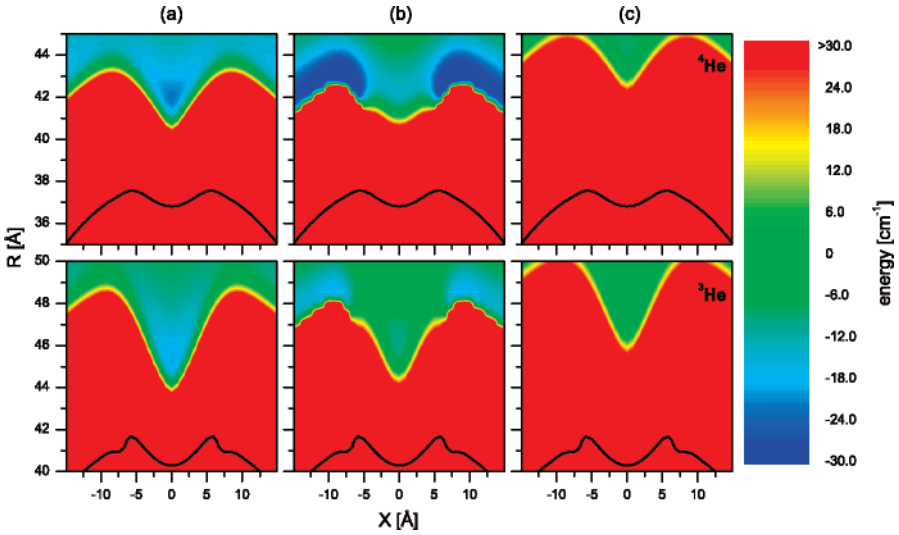

Figure 14. Two-dimensional potentials of (a) the ground state, (b) the Π state, and (c) the Σ state of lithium on $^4He_{5000}$ (upper panels) and $^3He_{5000}$ (lower panels) nanodroplets. *X* and *R* correspond to the position with respect to the droplet center. The black line represents the location of the droplet surface, see text for explanation.

here the Π transition should be dominated by a bound−bound transition. The simulations exactly confirm such a situation. The resulting absorption spectrum is plotted in Figure 12. The simulated spectrum reproduces the experimental one quite well, apart from the red-shifted shoulder. The maximum of the profile can be assigned to a transition into a bound Π state, the feature in the blue shoulder to the continuum transition of the Π and Σ states. The maxima of the simulated spectrum are again blue-shifted (Π, 5.5 cm^{-1}; Σ, 12 cm^{-1}).

The last calculated spectrum is for lithium on ^{3}He droplets. The results can be compared to the spectrum already presented in the experimental part of the paper. In contrast to ^{4}He, the experimental spectrum reveals that the second peak has more transition strength for ^{3}He (Figure 13). The same behavior is found in the simulation. The continuum part of the Π transition evolves enhanced transition strength. This leads to a rise of the second peak. Again a blue shift is observed (Π, 6 cm^{-1}; Σ, 9 cm^{-1}). Comparing ^{4}He and ^{3}He experimentally a blue shift less than 1 cm^{-1} is found. In perfect agreement the simulation predicts a blue shift of 1 cm^{-1}. The wide shoulder in the red is not reproduced by the simulation. This feature should have the same origin as the red shoulder in the case of lithium and sodium on ^{4}He droplets.

V. Discussion

The simulation nicely allows an assignment to all alkali metal spectra. Nearly all features in the absorption profiles can be correlated to a specific transition. In general, all simulated profiles are slightly blue-shifted compared to the experimental positions. This indicates a global effect that results in a red shift for all studied spectra. Stienkemeier et al. pointed out that the presence of a dielectric environment changes the radiative properties of atoms.[11] They found that the helium surface should lead to a red shift on the order of 9 cm^{-1}, which matches roughly our observations. For the Σ states we sometimes get larger shifts. Here a small change in the repulsive wall of the potential can lead to a huge shift in the absorption.

The obvious splitting of the $\Pi_{3/2}$ state, found in the experimental data, cannot be explained within the presented simulation. As already mentioned, experiments in bulk liquid helium also showed a splitting of the D_2 line of cesium and rubidium. In this case the problem has spherical symmetry and no orientation effects can lead to the observed splitting like that for the helium nanodroplets. Kinoshita et al. could explain the splitting via the dynamic Jahn−Teller effect due to a quadropole oscillation of the surrounding bubble.[18] They experimentally found a splitting of about 120 cm^{-1} (depending on the helium pressure), which was nicely reproduced in their theoretical model. One could imagine that the same effect is possible for a dimple structure. As a rough estimate, the splitting should scale with the size of the dimple, i.e., a residual half sphere results in half of the splitting. For cesium the dimple makes up one-third of a full sphere, meaning the splitting should be about a factor of 3 smaller than for the whole bubble. This value fits nicely the experimental findings, which showed a splitting of 49 cm^{-1}.

The last point to clarify is the origin of the red shoulder in the lithium and sodium spectra. These were not reproduced in the present simulation. The simulation was performed in only one dimension, moving the alkali metal atom along the atom−helium droplet "connecting" line. This limits the calculation to states that are located and vibrate along this axis, the symmetry axis. In principle, the atoms can also be located beyond this line and perform vibration perpendicularly to it. Such a state could in principle be lower in energy. To test the effect of the displacement *X* perpendicularly to the connecting line, we have calculated the interaction potential in two dimensions. Figure 14 shows the resulting potentials for the (a) ground, (b) Π, and (c) Σ state for lithium on ^{4}He and ^{3}He droplets with respect to the atomic asymptote. The upper panels presents the results for ^{4}He and the lower the ones for ^{3}He. The energy is displayed in false colors; green represents neither attraction nor repulsion. Blue indicates the attractive parts, and red the repulsive ones. The black line represents the position of the droplet surface, represented here by the equidensity line that corresponds to half of the bulk density value.

The ground state has its potential minimum located on the atom−droplet center connection line, as one would expect. The Σ state is purely repulsive. But for the Π state, attractive parts of the potential are found in the outer region of the dimple. For ^{4}He these are very pronounced with a well depth of ≈30 cm^{-1}, which nicely corresponds to the experimental red shift of the shoulder of 24 cm^{-1}. For ^{3}He, the attraction is much less with only a depth of ≈10 cm^{-1}, again in good agreement with the

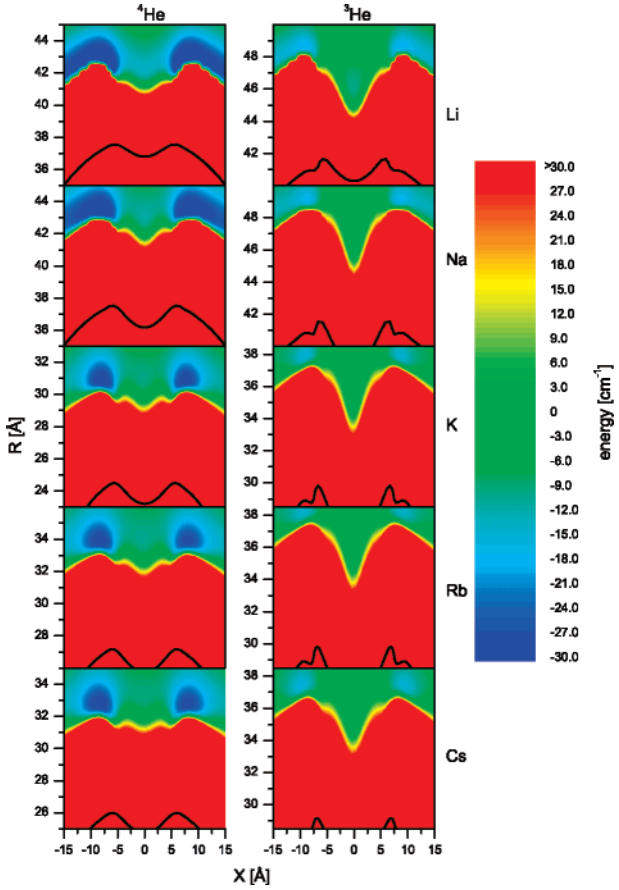

Figure 15. Two-dimensional potentials of the $\Pi_{3/2}$ state of Li(^{4}He$_{5000}$), Li(^{3}He$_{5000}$), Na(^{4}He$_{5000}$), Na(^{3}He$_{5000}$), K(^{4}He$_{1500}$), K(^{3}He$_{2000}$), Rb(^{4}He$_{2000}$), Rb(^{3}He$_{2000}$), Cs(^{4}He$_{2000}$), and Cs(^{3}He$_{2000}$). *X* and *R* correspond to the position with respect to the droplet center. The black line represents the location of the droplet surface, see text for explanation.

experimental findings. Due to the extend of the ground state potential well along the *X*-axis, overlap of these states with the ground state exists (cf. also the zero point motion of the light alkali metal atoms in the dimple calculated in ref 5).

Comparing the two-dimensional potential of the $\Pi_{3/2}$ states for all five investigated alkali metal atoms gives further support to our guessed explanation (Figure 15). Incorporating SO coupling leads to two Π states. Because of the spherical symmetry of the $\Pi_{1/2}$ state, the potential shows no attraction at the outer dimple region; only the $\Pi_{3/2}$ does. In the case of ^{4}He droplets all alkali metal atoms show an attractive part in the potential. The heavier the alkali metal atom, the less attractive it becomes. Additionally, its position moves to larger values of *X* and *R*, which results in a smaller overlap with the ground state. This illustrates that one expects no overlap of the ground state and the attractive part of the excited $\Pi_{3/2}$ state for the heavy alkali metal atoms. But for lithium, the sodium one can definitely reach them. For all ^{3}He potentials the attractive part is very weak and is located at much larger distances *R* with respect to the position of the ground state, making them no longer accessible. Hence, no red-shifted emission should be expected for ^{3}He droplets.

The shape of the dimple has a critical influence on the potential. As discussed before and shown in Figure 3, the depth of the dimple increases with the mass of the alkali metal atom, and it is larger for ^{3}He than for ^{4}He. In the case of a very shallow dimple, like the one for lithium on ^{4}He, a displacement of the p-orbital leads to only a small overlap with the helium density. If the dimple is much deeper, a lateral displacement results in a strong repulsive overlap. We thus conclude that the shape of the dimple is responsible for the red-shifted shoulder of the absorption spectrum, which is very sensitive to this shape. Hence, only shallow dimple states produce red-shifted shoulder states in the absorption profiles. These states correspond to vibrations along the surface of the helium droplets, which can in principle be modeled in full three-dimensional calculations.

VI. Summary and Outlook

We have presented in this paper new measurements of the 2p ← 2s transition of lithium on ^{3}He nanodroplets. With the help of a model calculation, the spectra of all stable alkali metal atoms on ^{4}He and ^{3}He droplets have been simulated. A comparison with the experimental findings has shown good agreement, and the different features of the spectra can be assigned to Π and Σ type transitions as well as to bound−bound and bound−unbound transitions. A general blue shift of the calculated profiles has been observed and has been attributed to the influence of the dielectric helium environment onto the electronic states of the alkali metal atoms.

With the help of a two-dimensional calculation of the interaction potentials, attractive parts of the Π state on the outer region of the dimple have been revealed. These are responsible for the red shoulder observed in the lithium and sodium spectra. To qualitatively support this finding three-dimensional calculations of the states and the resulting transitions have to be performed. These will be presented in a forthcoming paper.

Acknowledgment. We acknowledge stimulating discussions with Uwe Manthe (Universität Bielefeld) as well as Manuel Barranco (Universitat de Barcelona) for very helpful comments and advice. This work was financially supported by the DFG and by grants FIS2005-01414 from DGI, Spain, and 2005SGR00343 from Generalitat de Catalunya.

References and Notes

(1) Harms, J.; Hartmann, M.; Toennies, J. P.; Vilesov, A. F.; Sartakov, B. *J. Mol. Spectrosc.* **1997**, *5*, 204.
(2) Grebenev, S.; Toennies, J. P.; Vilesov, A. F. *Science* **1998**, *279*, 2083.
(3) Toennies, J. P.; Vilesov, A. F. *Angew. Chem.* **2004**, *43*, 2622.
(4) Stienkemeier, F.; Lehmann, K. K. *J. Phys. B* **2006**, *39*, R127.
(5) Barranco, M.; Guardiola, R.; Hernández, S.; Mayol, R.; Navarro, J.; Pi, M. *J. Low Temp. Phys.* **2006**, *142*, 1.
(6) Pascale, J. *Phys. Rev. A* **1983**, *28*, 632.
(7) Patil, S. H. *J. Chem. Phys.* **1991**, *94*, 8089.
(8) Partridge, H.; Stallcop, J. R. *J. Chem. Phys.* **2001**, *115*, 6471.
(9) Kleinekathöfer, U.; Lewerenz, M.; Mladenović, M. *Phys. Rev. Lett.* **1999**, *83*, 4717.
(10) Ancilotto, F.; Cheng, E.; Cole, M. W.; Toigo, F. *Z. Phys. B* **1995**, *98*, 323.
(11) Stienkemeier, F.; Higgins, J.; Callegari, C.; Kanorsky, S. I.; Ernst, W. E.; Scoles, G. *Z. Phys. D* **1996**, *38*, 253.
(12) Brühl, F. R.; Trasca, R. A.; Ernst, W. E. *J. Chem. Phys.* **2001**, *115*, 10220.
(13) Bünermann, O.; Mudrich, M.; Weidemüller, M.; Stienkemeier, F. *J. Chem. Phys.* **2004**, *121*, 8880.
(14) Stienkemeier, F.; Bünermann, O.; Mayol, R.; Ancilotto, F.; Barranco, M.; Pi, M. *Phys. Rev. B* **2004**, *70*, 214509.
(15) Mayol, R.; Ancilotto, F.; Barranco, M.; Bünermann, O.; Pi, M.; Stienkemeier, F. *J. Low Temp. Phys.* **2005**, *138*, 229.
(16) Takahashi, Y.; Sano, K.; Kinoshita, T.; Yabuzaki, T. *Phys. Rev. Lett.* **1993**, *71*, 1035.
(17) Kinoshita, T.; Fukuda, K.; Takahashi, Y.; Yabuzaki, T. *Phys. Rev. A* **1995**, *52*, 2707.
(18) Kinoshita, T.; Fukuda, K.; Yabuzaki, T. *Phys. Rev. B* **1996**, *54*, 6600.
(19) Enomoto, K.; Hirano, K.; Kumakura, M.; Takahashi, Y.; Yabuzaki, T. *Phys. Rev. A* **2004**, *69*, 012501.
(20) Hirano, K.; Enomoto, K.; Kumakura, M.; Takahashi, Y.; Yabuzaki, T. *Phys. Rev. A* **2003**, *68*, 012722.

(21) Enomoto, K.; Hirano, K.; Kumakura, M.; Takahashi, Y.; Yabuzaki, T. *Phys. Rev. A* **2002**, *66*, 042505.

(22) Nettels, D.; Hofer, A.; Moroshkin, P.; Müller-Siebert, R.; Ulzega, S.; Weis, A. *Phys. Rev. Lett.* **2005**, *94*, 063001.

(23) Moroshkin, P.; Hofer, A.; Nettels, D.; Ulzega, S.; Weis, A. *J. Chem. Phys.* **2006**, *124*, 024511.

(24) Eichler, T.; Müller-Siebert, R.; Nettels, D.; Kanorsky, S.; Weis, A. *Phys. Rev. Lett.* **2002**, *88*, 123002.

(25) Reho, J.; Callegari, C.; Higgins, J.; Ernst, W. E.; Lehmann, K. K.; Scoles, G. *Faraday Discuss.* **1997**, *108*, 161.

(26) Reho, J.; Higgins, J.; Callegari, C.; Lehmann, K. K.; Scoles, G. *J. Chem. Phys.* **2000**, *113*, 9686.

(27) Reho, J.; Higgins, J.; Callegari, C.; Lehmann, K. K.; Scoles, G. *J. Chem. Phys.* **2000**, *113*, 9694.

(28) Schulz, C. P.; Claas, P.; Stienkemeier, F. *Phys. Rev. Lett.* **2001**, *87*, 153401.

(29) Droppelmann, G.; Bünermann, O.; Schulz, C. P.; Stienkemeier, F. *Phys. Rev. Lett.* **2004**, *93*, 023402.

(30) Stienkemeier, F.; Meier, F.; Lutz, H. O. *Eur. Phys. J. D* **1999**, *9*, 313.

(31) Stienkemeier, F.; Wewer, M.; Meier, F.; Lutz, H. O. *Rev. Sci. Instrum.* **2000**, *71*, 3480.

(32) Hernando, A.; Mayol, R.; Pi, M.; Barranco, M.; Ancilotto, F.; Bünermann, O.; Stienkemeier, F. *J. Phys. Chem. A* **2007**.

(33) Kerkines, I. S. K.; Mavridis, A. *J. Phys. Chem. A* **2000**, *104*, 408.

(34) Leo, P. J.; Peach, G.; Whittingham, I. B. *J. Phys. B* **2000**, *33*, 4779.

(35) Santra, R.; Kirby, K. *J. Chem. Phys.* **2005**, *123*, 214309.

(36) Alexander, M. H.; Walton, A. R.; Yang, M.; Yang, X.; Hwang, E.; Dagdigian, P. J. *J. Chem. Phys.* **1997**, *106*, 6320.

(37) Cohen, J. S.; Schneider, B. *J. Chem. Phys.* **1974**, *61*, 3230.

(38) Zare, R. N. *Angular Momentum*; Wiley: New York, 1988.

(39) Roy, R. J. L. Level 8.0: A computer program for solving the radial Schrödinger equation for bound and quasibound levels, University of Waterloo, 2007.

(40) Roy, R. J. L.; Kraemer, G. T. Bcount 2.2: A computer program for calculating bound → continuum transition intensities for diaatomic molecules, University of Waterloo,, 2004.

(41) Placing the alkali metal off-axis leads to a breaking of the cylindrical symmetry of the system. In this case, the off-diagonal elements cannot be neglected. We expect the error to be small. Only a full 3-dimensional calculation would be appropriate to completely circumvent this problem.